

## Anomalous electron mobility in a coaxial Hall discharge plasma

Nathan B. Meezan, William A. Hargus, Jr., and Mark A. Cappelli

*Mechanical Engineering Department, Stanford University, Stanford, California 94305-3032*

(Received 12 June 2000; published 24 January 2001)

A comprehensive analysis of measurements supporting the presence of anomalous cross-field electron mobility in Hall plasma accelerators is presented. Nonintrusive laser-induced fluorescence measurements of neutral xenon and ionized xenon velocities, and various electrostatic probe diagnostic measurements are used to locally determine the effective electron Hall parameter inside the accelerator channel. These values are then compared to the classical (collision-driven) Hall parameters expected for a quiescent magnetized plasma. The results indicate that in the vicinity of the anode, where there are fewer plasma instabilities, the electron-transport mechanism is likely elastic collisions with the background neutral xenon. However, we find that in the vicinity of the discharge channel exit, where the magnetic field is the strongest and where there are intense fluctuations in the plasma properties, the inferred Hall parameter departs from the classical value, and is close to the Bohm value of  $(\omega_{ce}\tau)_{\text{eff}} \approx 16$ . These results are used to support a simple model for the Hall parameter that is based on the scalar addition of the electron collision frequencies (elastic collision induced plus fluctuation induced), as proposed by Boeuf and Garrigues [J. Appl. Phys. **84**, 3541 (1998)]. The results also draw attention to the possible role of fluctuations in enhancing electron transport in regions where the electrons are highly magnetized.

DOI: 10.1103/PhysRevE.63.026410

PACS number(s): 52.25.Fi, 52.75.Di, 52.70.Ds, 52.70.Kz

### I. INTRODUCTION

The use of coaxial Hall discharges as high specific impulse plasma accelerators for satellite propulsion date back to the early 1960's. In a Hall discharge (Fig. 1), the plasma is sustained in imposed orthogonal electric and magnetic fields. The discharge electrons, a large fraction of which are emitted by an external cathode, are magnetized, whereas the more massive propellant ions, usually xenon, are not. Consequently, the electrostatic fields established by the retarded electron flow accelerate the ions to high velocities, typically 50%–60% of the discharge voltage. In a coaxial geometry, the electrons are constrained to move in the closed, azimuthal  $\mathbf{E} \times \mathbf{B}$  drift, with cross-field diffusion providing the necessary current to sustain the discharge.

The first detailed investigation of the properties of these coaxial Hall discharges suggested that the axial electron current density is greater than that expected by classical transport [1]. This led to the first speculation of the presence of an “anomalous” cross-field drift of electrons, due in part to fluctuations in the electric field and plasma density. Fluctuations in the external circuit and plasma properties in these devices are now well documented [2–5], and recent numerical simulations of Hall discharges generally require the *ad hoc* introduction of an anomalous electron mobility to produce reasonably accurate results [6–9]. Despite many experimental and theoretical studies, the precise nature of the instabilities responsible for these fluctuations and the mechanism for their excitation are not yet well understood. Furthermore, other mechanisms, including collisions between energetic electrons and the channel wall, and experimental facility effects such as background gas ingestion may also play important roles in electron transport.

In this paper, we examine the electron-transport mechanism in a coaxial Hall discharge through a collection of applied diagnostics that serve to map the electron mobility in

the discharge channel. The two-dimensional electron momentum equation for a weakly ionized plasma gives the electron current density,

$$J_{ez} = en_e u_{ez} = en_e \left( \frac{E_z}{B_r} \right) \frac{\nu_{ne}}{\omega_{ce}} = en_e \left( \frac{E_z}{B_r} \right) \frac{1}{\omega_{ce} \tau}. \quad (1)$$

Here,  $n_e$  is the electron density,  $u_{ez}$  is the electron drift velocity,  $\nu_{ne}$  is the momentum-transfer collision frequency for neutral-electron collisions,  $\tau$  is the mean time between collisions, and the electron cyclotron frequency  $\omega_{ce} \gg \nu_{ne}$ . It is assumed that the applied electric field  $E_z$  and magnetic field strength  $B_r$  are in the axial and radial directions, respec-

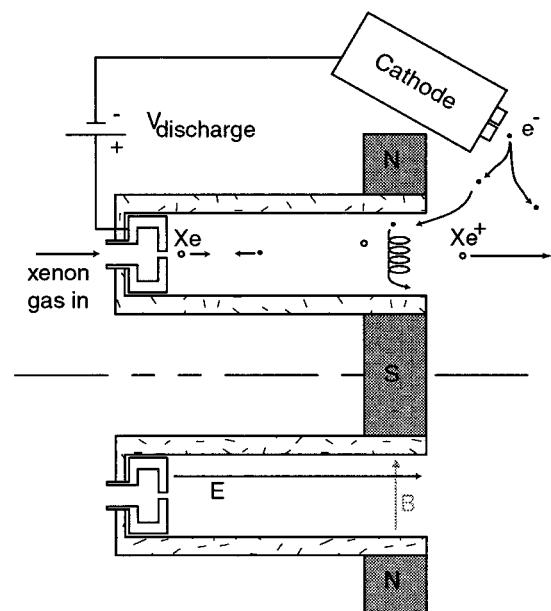


FIG. 1. Schematic of a typical Hall discharge accelerator.

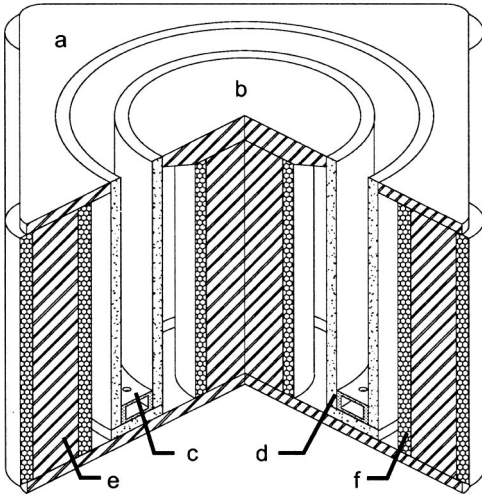


FIG. 2. Cutaway schematic of the Hall discharge studied. (a) Front magnetic plate; (b) central magnetic plate; (c) anode gas input; (d) alumina insulator wall; (e) magnet core; and (f) magnetic windings.

tively. From Eq. (1), we see that the cross-field electron mobility is inversely proportional to the electron Hall parameter,  $\omega_{ce}\tau$ ,

$$\mu_{ez} = \left( \frac{1}{B_r} \right) \frac{1}{\omega_{ce}\tau}. \quad (2)$$

Equation (1) can be rearranged to give

$$\frac{1}{(\omega_{ce}\tau)} = \left( \frac{B_r}{E_z} \right) \frac{J_{ez}}{en_e}. \quad (3)$$

The Hall parameter (or electron mobility) can therefore be determined at any point in the discharge channel where the plasma properties on the right-hand side of Eq. (3) are known. Furthermore, the resulting Hall parameter can be compared to that calculated on the basis of known properties that independently determine the electron cyclotron frequency and the mean time between electron collisions. In this paper, we review our recent experimental measurements of plasma properties within the discharge channel, which permit this direct comparison. The results support the presence of an anomalous transport mechanism in regions of the plasma known to support fluctuations, and provide the first direct quantitative measure of the axial variation in the electron mobility.

## II. EXPERIMENTS

### A. Prototype Hall discharge

The Hall plasma source studied here was constructed at Stanford as a test bed for studying the discharge physics and is not intended to serve as an operational prototype plasma accelerator. A cutaway schematic of the plasma source is shown in Fig. 2. The source consists of an annular alumina channel 90 mm in diameter, 11 mm in width, and 80 mm in length. A magnetic circuit consisting of four outer coils, one

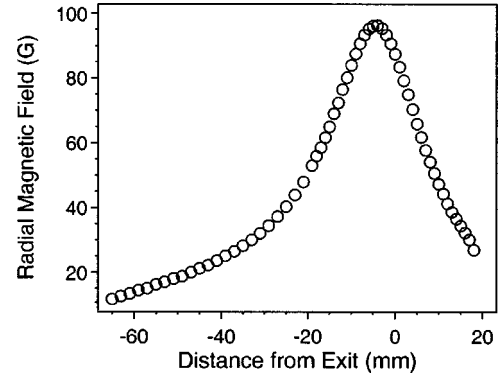


FIG. 3. Axial profile of radial magnetic-field strength for the Hall discharge studied.

inner coil, and three iron plates provides a magnetic field (mostly radial in direction) peaked near the exit of the discharge channel, as shown in Fig. 3. A hollow stainless-steel ring with 32 holes of 0.5-mm diameter serves both as the anode and the propellant (gas) input of the discharge.

A commercial hollow cathode (Ion Tech HCN-252) is used to neutralize the resulting ion beam and support the necessary electric field. The cathode is mounted approximately 2 cm downstream of the plasma source exit. The cathode body was kept at the vacuum chamber ground potential. To allow optical and probe access inside the discharge channel, a 1 mm wide slot was cut along the outer insulator wall, parallel to the discharge axis. The performance of the discharge is not noticeably altered by the presence of the slot.

Two independent mass flow controllers control the gas flow to the anode and cathode. Direct current power supplies are used to independently power the discharge, cathode heater, cathode keeper, and magnetic windings. The discharge (anode) power supply is always operated in the voltage-regulated limit. The experimental facility consists of a nonmagnetic stainless-steel tank approximately 1 m in diameter and 1.5 m in length pumped by two 50-cm diameter diffusion pumps and backed by a 425 L/s mechanical pump. The facility is equipped with several viewports and feedthroughs for optical and probe access to the discharge. The base pressure of the facility with no gas flow is approximately  $10^{-6}$  Torr as measured by an ionization gauge uncorrected for gas species. The background pressure during discharge operation at a xenon flow rate of 2.3 mg/s is typically  $10^{-4}$  Torr. Although this pressure is an order of magnitude lower than that of Janes and Lowder [1], it is still considerably higher than chamber pressures that are generally acceptable for the collection of accelerator performance data [10,11]. The ingestion of background gas near the exit of the discharge channel may influence the discharge characteristics.

### B. Plasma diagnostic techniques

A variety of optical and probe diagnostics were utilized to measure the plasma properties needed for the determination of the effective Hall parameter [using Eq. (3)]. The potential distribution in the discharge was measured using an emissive

probe. This technique is described in more detail in another paper [12], and is only briefly summarized here. A tungsten filament inserted into the discharge channel was heated using a variable-current alternating current (ac) power supply and a second, floating step-down transformer. The filament current was increased until the potential of the floating transformer with respect to ground reached a nearly saturated value. This value was taken as the plasma potential [13]. This method of finding the plasma potential is less accurate than the more common ‘‘inflection point’’ method [14]; however, this alternative method involves the collection of electron current by the probe. Due to the small size of the discharge channel, it has been our experience that collecting electrons from the plasma can severely perturb the operation of the discharge. A probe collecting electron current causes a much greater disturbance on discharge performance than a floating probe or one collecting ion current. The floating potential of the plasma was also recorded at each point using the same probe without current passing through the filament. The magnetic-field distribution inside the channel was measured with the discharge off using a Hall effect sensor probe.

The electron current density is determined from the total discharge current density (discharge current divided by the channel cross sectional area) less the ion current density:

$$J_{ez} = I/A_{\text{channel}} - n_e V_i. \quad (4)$$

The ion current density is determined either directly using a guarded ion flux probe, or from a measurement of the electron (ion) density using a cylindrical Langmuir probe (discussed below) and from laser-induced fluorescence (LIF) measurements of the xenon ion velocity. These LIF measurements are described in detail elsewhere [12,15]. They involve propagating a narrow-linewidth, continuous-wave laser beam through the plasma along the discharge axis and measuring the fluorescence signal as a function of laser frequency. Due to the Doppler effect, the absorption line center is shifted from that of a stationary plasma reference. The bulk velocity of the absorbing xenon ions can then be determined from this frequency shift. In the studies reported here, a Coherent 899-21 tunable titanium sapphire laser was used to excite the  $5d[4]_{7/2} - 6p[3]_{5/2}$  transition in Xe II at 834.7 nm, with nonresonance fluorescence detected at 541.9 nm. A similar method was also used to measure the velocity of excited neutral xenon atoms using the  $6s[\frac{3}{2}]_2^0 - 6p[\frac{3}{2}]_2$  transition at 823.2 nm, only in this case, resonance fluorescence is detected. The neutral atom velocity together with the overall xenon mass flow rate served to provide a measure of the neutral xenon number density, from which the classical Hall parameter can be determined.

The electron density in the discharge was measured using two different techniques. In the first set of experiments, a cylindrical Langmuir probe was inserted into the discharge channel through the optical access slot. The probe was a 0.5-mm diameter tungsten wire bent at a right angle so that a 5-mm length of the probe was parallel to the ion flow in the channel. The ion-saturation current was collected at a probe bias of  $-46$  V and the electron (ion) density was determined using a thin (‘‘free-fall’’) sheath approximation [16] for ion

collection. This required an estimate of the electron temperature, as described below. Inserting the probe through the access slot minimized its disturbance of the plasma, but also prevented measurements near the exit of the discharge.

Shortcomings of this probe characterization method included spatial averaging along the length of the probe, ‘‘shadowing’’ of the backside of the probe due to wake formation, and the use of a relatively simple ion current collection theory for a high-velocity plasma in the presence of a magnetic field. The effects of the magnetic field on particle collection by the probe can be measured through the electron and ionic Larmor radii. For the Hall discharge,  $r_e \approx a$  and  $r_i \gg w \gg a$ , where  $r_e$  and  $r_i$  are the electronic and ionic Larmor radii,  $a$  is the probe radius, and  $w$  is the channel width. While electron collection will be affected by the magnetic field, the ions are essentially not magnetized. Therefore, as pointed out by Batani *et al.* [17], the effect of the magnetic field on a measurement of the electron density from the ion current will be negligible compared to the 20% accuracy expected by this probe theory. Ideally, the entire Langmuir probe trace would be used for determining the electron temperature, plasma density, and plasma potential. As mentioned above, scanning the probe voltage into the electron-collection region is not desirable in this discharge, as it may strongly perturb the plasma, and requires an appropriate theoretical treatment of probe traces when electrons are strongly magnetized.

As mentioned above, the ion current density is also determined directly using a guarded ion-flux probe [18]. The ion (hence electron) density can be determined from these probe measurements and the measurements of the ion velocity. The ion probe was constructed of 1.5-mm diameter tungsten rod surrounded by an alumina sleeve. A tantalum guard ring biased to the same potential as the probe was mounted around the center probe to establish a one-dimensional sheath across the probe collection area, and to minimize outer sheath collection area growth with probe bias. At all locations within the discharge, the probe was biased at 20 V below the local floating potential. It is noted, however, that inserting the probe into the discharge channel caused a significant increase in the total discharge current, up to 20%. The intrusive perturbation of this probe precluded measurements upstream of the discharge exit plane.

Measurements of plasma fluctuations were also made to give insight into the role of oscillations in electron transport. Low-impedance shielded Langmuir probes were used to measure fluctuations in ion-saturation current, which roughly correspond to fluctuations in plasma density. These probes were designed to detect propagating plasma waves in the Hall discharge, experiments described in great detail in another paper [19]. For this experiment, one probe was connected to a direct current (dc) coupled digital oscilloscope through a 50  $\Omega$  terminator. Due to the high floating potential inside the discharge, this grounded probe collected current in the ion-saturation regime of the Langmuir probe trace.

### III. RESULTS AND ANALYSIS

The plasma potential profiles as measured by the hot-filament probe are shown in Fig. 4 for the three operating

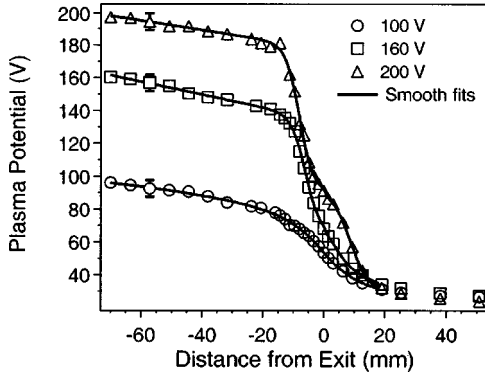


FIG. 4. Plasma potential profiles measured by the emissive probe.

conditions investigated in this paper. The floating potential of an emitting probe should be slightly below the actual plasma potential, since the emission will never be enough to neutralize the sheath [14]. It can be seen from Fig. 4 that as the probe approaches the anode, the measured plasma potential comes quite close to the applied anode potential. With the probe 5 mm away from the anode, the measured values are within 4 V of the applied potential, suggesting that the uncertainty in the measured potential is within 5 V, and possibly less, depending on the strength of the anode fall. The electric field inside the discharge channel, shown in Fig. 5, was calculated from the plasma potential data using the relation  $E_z = -d\phi/dz$ . Smooth curves were fit to the potential profiles before differentiation to prevent noise amplification. It is noteworthy that the peak in the electric field coincides closely with the peak in the magnetic field, although the distribution is more narrow, suggesting that the electron  $\mathbf{E} \times \mathbf{B}$  drift velocity,  $u_d = E_z/B_r$ , is also highly peaked near  $z = -10$  mm.

The plasma potential data was used in conjunction with floating potential data (not shown) to calculate the electron temperature:

$$\phi_p - \phi_f = \frac{kT_e}{2e} \ln\left(\frac{m_i}{2\pi m_e}\right). \quad (5)$$

Here, we assume that the ions enter the sheath at the Bohm velocity.

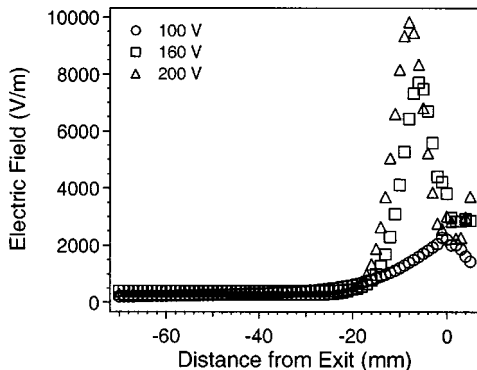


FIG. 5. Electric-field profiles calculated from plasma potential.

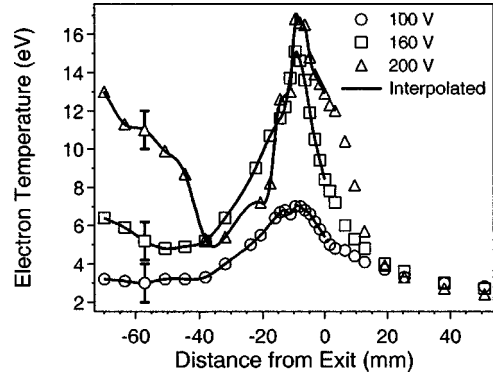


FIG. 6. Electron temperature profiles calculated from plasma and floating potential data.

The electron temperature is shown in Fig. 6. These temperature profiles are used in the remaining calculations needed to estimate the Hall parameter. The electron temperature is seen to peak above 16 eV. Although the temperature could be in error by a few volts due to underestimation of the plasma potential, the measured values do agree well with those from other investigators in similar discharges [20,21]. The peak in the electron temperature is coincident with the peaks in the electric and magnetic fields, as expected since the Ohmic dissipation will scale as  $J_{ez}E_z$ . We see an unexpected rise in the electron temperature near the anode for the higher power cases studied, most likely due to the formation of an anode glow region, as the production of electrons is needed in this region to support the higher current densities. These striking distributions suggest that the discharge length is not optimized, and can be shortened to 40 mm for more efficient operation as a plasma accelerator at the higher-voltage conditions.

The electron temperature is used to determine the electron (ion) density from the ion saturation current collected with the Langmuir probe discussed above,

$$J_{is} = 0.61en_e \sqrt{\frac{kT_e}{m_i}}. \quad (6)$$

The electron-density profiles measured from the two probe methods are plotted together in Fig. 7. As mentioned above, the error in the electron temperature will have a small impact on this measurement. For example, an error as large as 2 eV

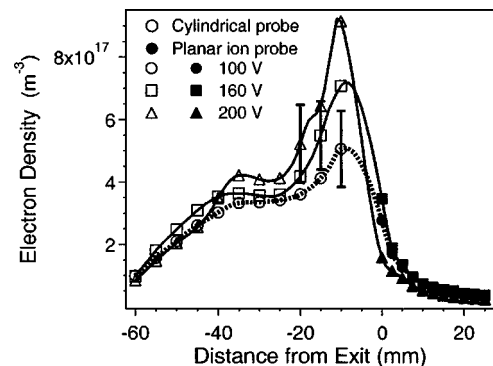


FIG. 7. Electron-density profiles from probe experiments.

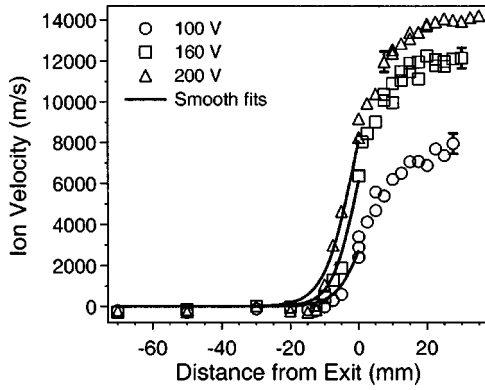


FIG. 8. Ion velocity profiles measured by laser-induced fluorescence velocimetry.

in a measured electron temperature of 6 eV will lead to an error of 15%–20% in the electron density—within the expected accuracy of the method.

The intrusive nature of the guarded ion probe precluded measurements with this probe within the discharge channel. Furthermore, the Langmuir probe inserted through the slot in the insulator was unable to collect data within a distance of 10 mm upstream of the channel exit, because of the presence of the magnetic pole piece. As a result, the two probe measurements were indeed complementary, and a cubic-spline interpolation was used to estimate the plasma density in the range between the discharge channel exit and the location of the base of the front magnetic plate. The resultant spline fits are also shown in Fig. 7. The electron number densities are seen to peak in the same vicinity where the other plasma properties reach their maximum values. The error in the electron-density measurement inside the channel is quite significant, but it is also bound. The values have an upper bound of 100% propellant utilization (i.e., the ion flow leaving the channel equals the mass flow entering the channel), and the ion-flux measurements effectively provide a lower bound on the density near the exit plane.

The ion velocity profiles measured using LIF are shown in Fig. 8. Just downstream of the high-temperature ionization region, the produced ions are seen to accelerate to high velocities consistent with the measured plasma potential distributions.

The data given above for  $B_r$ ,  $E_z$ ,  $n_e$ , and  $V_i$  (ion velocity) is enough to calculate the effective Hall parameter along the Hall discharge channel from Eqs. (3) and (4). This Hall parameter can be compared to the “classical” Hall parameter expected based on the electron momentum-transfer collision frequency  $\nu_{ne}$ . For this calculation, the neutral gas density (the dominant electron collision partner) is determined from the neutral xenon velocity data, shown in Fig. 9, and the discharge mass flow rate,

$$n_g = \left( \frac{\dot{m}}{m_i A_{\text{channel}}} - n_e V_i \right) \frac{1}{V_n}. \quad (7)$$

The axial variation in the inferred neutral density is shown in Fig. 10.

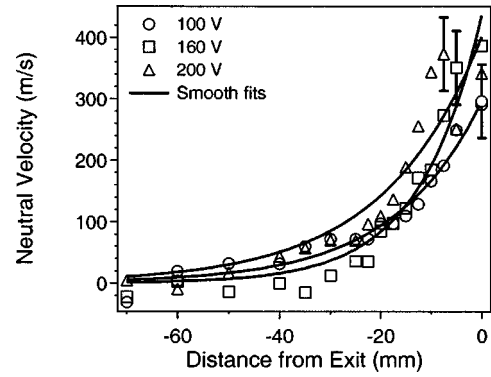


FIG. 9. Neutral xenon velocity profiles measured by laser-induced fluorescence velocimetry.

The dip in the neutral density near the exit plane at higher discharge voltages is due to the measurement of a significant increase in the ion flux, reflecting the ionization process taking place between  $z = -5$  and  $z = -10$  mm. It is noteworthy that the calculation of the neutral gas density does not take ingestion of background gas from the vacuum chamber into account. Background chamber neutral xenon ingestion would cause an underestimate of the neutral xenon density, as the actual mass flow rate would be higher. These measurements of xenon density should be interpreted as lower limits on the actual values.

The electron momentum-transfer collision frequency was calculated using the cross section given in the SIGLO© database [22] assuming a Maxwellian electron energy distribution, using the electron temperature measurements described above.

#### IV. DISCUSSION

The deduced Hall parameter is compared to the “classical” Hall parameter (that determined by the direct calculation of the electron momentum-transfer collision frequency), in Fig. 11. In the figure, we plot the inverse of the Hall parameter ( $1/\omega_{ce}\tau$ ), since this is proportional to the electron cross-field mobility [see Eq. (2)].

It is apparent from Fig. 11 that elastic electron-neutral collisions are the likely mechanisms for cross-field electron transport at locations between the anode ( $z = -80$  mm) and

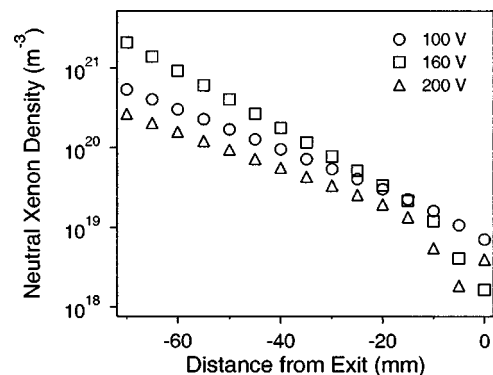


FIG. 10. Neutral xenon density profiles.

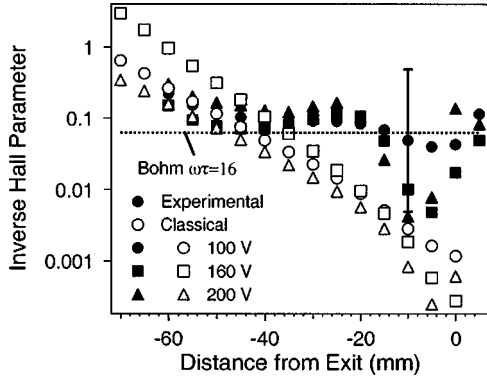


FIG. 11. Effective and classical inverse Hall parameter profiles inside Hall discharge channel.

approximately 40 mm upstream of the discharge channel exit. It is noteworthy that this location is where the magnetic-field strength reaches approximately 1/5th of its peak value (see Fig. 3). We also see that beyond this location, there is a striking departure from this classical value, although the uncertainty in the absolute measurements is still significant, a result mainly attributable to the uncertainty in the total discharge current caused by the intrusive nature of the diagnostic probes. At locations downstream of the  $z = -40$  mm position, where the magnetic field reaches a maximum, the inverse Hall parameter is in remarkable agreement with the Bohm value of  $\omega_{ce}\tau = 16$  [23]. In this region, we [24–28], and others [2–5,29–32] have reported on the existence of intense fluctuations in the plasma properties. These results are supportive of the conjecture that plasma fluctuations are partially responsible for the anomalous cross-field transport, although additional experiments may be necessary to obtain more accurate quantitative measurements of the resulting mobility. The results reported on here do, however, provide the first direct support of a model based on the use of a “mixed” mobility (or collision frequency),

$$\left(\frac{1}{\omega_{ce}\tau}\right)_{\text{total}} = \left(\frac{1}{\omega_{ce}\tau}\right)_{\text{collisions}} + \left(\frac{1}{\omega_{ce}\tau}\right)_{\text{oscillations}}, \quad (8)$$

as has been originally proposed by Boeuf and Garrigues for numerical simulations of Hall discharges [7]. The Bohm

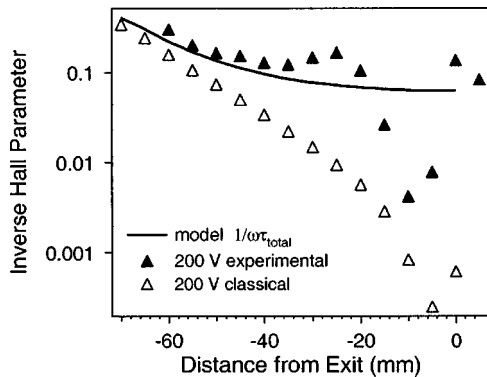


FIG. 12. Comparison of mixed mobility model to experimental and classical inverse Hall parameter profiles at 200 V operation.

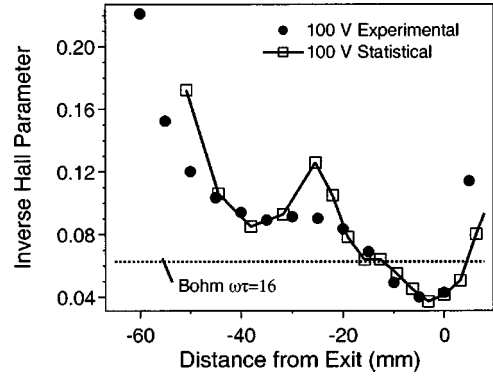


FIG. 13. Comparison of statistical fluctuation analysis to experimental inverse Hall parameter profile at 100 V operation.

value appears to be reasonable for the oscillation-induced part of the mobility (Fig. 12), despite the lack of a full understanding of the instabilities in this region of the plasma.

Additional support for the conjecture that oscillations are at least partly responsible for the enhanced cross-field mobility can be found in statistical analysis of probe fluctuation data. For a homogeneous plasma subjected to homogeneous turbulent fluctuations in the plasma density, the cross-field electron diffusion coefficient (which is directly proportional to the inverse of the effective Hall parameter) can be expressed as [33]

$$D_{\perp} \propto \frac{1}{(\omega\tau)_{\text{eff}}} = \frac{\pi}{4} \left[ \frac{\langle (n_e - \langle n_e \rangle)^2 \rangle}{\langle n_e \rangle^2} \right]. \quad (9)$$

The quantity inside the square brackets is the mean-square deviation of the observed plasma density fluctuation. As mentioned above, the raw fluctuation data collected by an ion-current probe is proportional to the local plasma density. Equation (9) was therefore applied directly to the raw probe data inside the discharge channel. This “statistical Hall parameter” is compared to the experimental value in Fig. 13. The agreement is remarkable, although the uncertainty in the measured value of the Hall parameter is large. More significantly, the trend in the mean-square deviation of the plasma density follows the experimental value very closely, suggesting that the role of fluctuations may be important.

The relatively large error bars in Fig. 11 are a consequence of the number of different data used to calculate the Hall parameter. The largest source of error is the measurement of the total current through the discharge. At a given voltage, the current through the discharge used in this study can drift up to 10% in a half hour, presumably due to fluctuations in the facility background pressure. Furthermore, the insertion of the ion and/or Langmuir probe gives rise to a perturbation that can be as high as 20% on the total discharge current. An alternate, nonintrusive measurement of the electron density is favored, and is the subject of our present research. Efforts will also be made to reduce the perturbation caused by the emissive potential probe.

## V. CONCLUSIONS

In this paper, we have used a variety of plasma diagnostic techniques, both intrusive and nonintrusive, to evaluate the effective electron mobility in a Hall discharge. We provide strong evidence of the presence of an anomalous transport mechanism, in the region of the plasma where there is a strong radial magnetic field, and where we have seen intense plasma fluctuations. The Hall parameter has been shown to approach a constant value, within the margin of error, near the Bohm value of 16 in this region. Although these results fall short of identifying fluctuations in plasma density and/or temperature as the source of this enhanced cross-field electron mobility, they do suggest that fluctuations in plasma properties can account for the observed axial electron current flow. The Hall discharge accelerator falls within a difficult regime for plasma diagnostics—the device is small, low-density, fluctuating, and magnetized, making it difficult to interpret probe-based measurements of electron density using available probe theory. Furthermore, although the electron-density measurements themselves are not the largest source of uncertainty, we find that the probes used for these measurements have a weak perturbing effect on the total dis-

charge current, which does strongly contribute to the measurement accuracy. Future studies will focus on the development of nonintrusive measurements of plasma density to improve the measurement accuracy.

The most significant finding is that the results are in remarkable agreement with a simple model for the Hall parameter that is based on the scalar addition of the electron collision frequencies (elastic collision induced plus fluctuation induced), as first proposed by Boeuf and Garrigues [7]. The transition from a fluctuation-dominated mobility (Bohm-like) to collision induced mobility is found to occur at the point where the magnetic field is approximately 20% of its peak value, and where our other studies [19,28] identify the spatial onset of strong, quasicohherent azimuthally propagating waves in plasma density and potential.

## ACKNOWLEDGMENTS

This work was supported by the Air Force Office of Scientific Research. W. Hargus Jr. was supported by the Air Force Palace Knight Program. The authors acknowledge the technical assistance of D. P. Schmidt.

- 
- [1] G. S. Janes and R. S. Lowder, *Phys. Fluids* **9**, 1115 (1966).
  - [2] A. I. Morozov *et al.*, *Zh. Tekh. Fiz.* **42**, 612 (1972) [*Sov. Phys. Tech. Phys.* **17**, 482 (1972)].
  - [3] Y. B. Esipchuk *et al.*, *Zh. Tekh. Fiz.* **43**, 1466 (1973) [*Sov. Phys. Tech. Phys.* **18**, 928 (1973)].
  - [4] E. Y. Choueiri, AIAA Paper No. 94-3013, *30th Joint Propulsion Conference, Indianapolis, IN, 1994* (American Institute of Aeronautics and Astronautics, Washington, DC, 1994).
  - [5] G. Guerrini and C. Michaut, *Phys. Plasmas* **6**, 343 (1999).
  - [6] J. Fife and M. Martinez-Sanchez, AIAA Paper No. 96-3197, *32nd Joint Propulsion Conference, Lake Buena Vista, FL, 1996*.
  - [7] J. P. Boeuf and L. Garrigues, *J. Appl. Phys.* **84**, 3541 (1998).
  - [8] J. J. Szabo, Jr. and M. Martinez-Sanchez, AIAA Paper No. 98-3795, *34th Joint Propulsion Conference, Cleveland, OH, 1998*.
  - [9] E. Ahedo and M. Martinez-Sanchez, AIAA Paper No. 98-3788, *34th Joint Propulsion Conference, Cleveland, OH, 1998*.
  - [10] T. Randolph *et al.*, IEPAC Paper No. 93-093, *23rd International Electric Propulsion Conference, Seattle WA, 1993*.
  - [11] S. C. Bechu *et al.*, AIAA Paper No. 99-2567, *35th Joint Propulsion Conference, Los Angeles, CA, 1999*.
  - [12] W. A. Hargus, Jr. and M. A. Cappelli, AIAA Paper No. 99-2721, *35th Joint Propulsion Conference, Los Angeles, CA, 1999*.
  - [13] F. F. Chen, in *Plasma Diagnostic Techniques*, edited by R. H. Huddlestone and S. L. Leonard (Academic, New York, 1965), Chap. 4, p. 184.
  - [14] J. R. Smith, N. Hershkowitz, and P. Coakley, *Rev. Sci. Instrum.* **50**, 210 (1979).
  - [15] R. J. Cedolin, W. A. Hargus, Jr., and M. A. Cappelli, *Appl. Phys. B: Photophys. Laser Chem.* **65**, 459 (1997).
  - [16] A. Lieberman and A. J. Lichtenberg, *Principles of Plasma Discharges and Materials Processing* (Wiley, New York, 1994), p. 174.
  - [17] D. Batani *et al.*, *Rev. Sci. Instrum.* **68**, 4043 (1997).
  - [18] G. S. Janes and J. P. Dotson, *Rev. Sci. Instrum.* **8**, 284 (1964).
  - [19] E. Chesta *et al.* (unpublished).
  - [20] M. Bishaev and V. Kim, *Zh. Tekh. Fiz.* **48**, 1853 (1978) [*Sov. Phys. Tech. Phys.* **23**, 1055 (1978)].
  - [21] A. I. Bugrova *et al.*, *Teplofiz. Vys. Temp.* **19**, 1149 (1981) [*High Temp.* **19**, 822 (1981)].
  - [22] CPAT and Kinema Software, [www.csn.net/siglo](http://www.csn.net/siglo) (1998).
  - [23] D. Bohm, in *The Characteristics of Electrical Discharges in Magnetic Fields*, edited by A. Guthrie and R. K. Wakerling (McGraw-Hill, New York, 1949), Chap. 2, p. 65.
  - [24] M. A. Cappelli, W. A. Hargus, Jr., and N. B. Meezan, *IEEE Trans. Plasma Sci.* **27**, 96 (1999).
  - [25] N. B. Meezan and M. A. Cappelli, AIAA Paper No. 98-3502, *34th Joint Propulsion Conference, Cleveland, OH, 1998*.
  - [26] N. B. Meezan and M. A. Cappelli, AIAA Paper No. 99-2284, *35th Joint Propulsion Conference, Los Angeles, CA, 1999*.
  - [27] D. P. Schmidt, N. B. Meezan, and M. A. Cappelli, AIAA Paper No. 99-3437, *30th Plasmadynamics and Lasers Conference, Norfolk, VA, 1999*.
  - [28] E. Chesta, N. B. Meezan, and M. A. Cappelli (unpublished).
  - [29] F. Darnon *et al.*, *IEEE Trans. Plasma Sci.* **27**, 98 (1999).
  - [30] N. Gascon *et al.*, AIAA Paper No. 99-2427, *35th Joint Propulsion Conference, Los Angeles, CA, 1999*.
  - [31] D. Pagnon *et al.*, AIAA Paper No. 99-2428, *35th Joint Propulsion Conference, Los Angeles, CA, 1999*.
  - [32] G. Guerrini and C. Michaut, *Phys. Plasmas* **6**, 343 (1999).
  - [33] S. Yoshikawa and D. J. Rose, *Phys. Fluids* **5**, 334 (1962).